ChemComm

Dirhodium Complexes as Electrocatalysts for CO2 Reduction to HCOOH: Role of Steric Hindrance on Selectivity

Journal:	*ChemComm*
Manuscript ID	CC-COM-11-2020-007659.R1
Article Type:	Communication

COMMUNICATION

Dirhodium Complexes as Electrocatalysts for CO_2 Reduction to HCOOH: Role of Steric Hindrance on Selectivity

Hemanthi D. Manamperi, [a] Curtis E. Moore [a] and Claudia Turro *[a]

Received 00th January 20xx,
Accepted 00th January 20xx

DOI: 10.1039/x0xx00000x

A series of Rh_2(II,II) complexes were shown to electrocatalytically reduce CO_2 to HCOOH. Electrochemical and spectroelectrochemical studies reveal a correlation between catalytic selectivity and efficiency with the steric bulk at the axial sites afforded by the bridging ligands. Mechanistic studies point to the presence of a Rh_2(II,I)-H hydride as a key intermediate in the catalytic cycle.

Carbon dioxide is an ideal C1 feed stock to generate products that store energy in the form of chemical bonds or generate value-added chemicals.[1-3] However, the high stability of CO_2 makes its reduction challenging, such that the generation of useful products often requires multi-electron/multi-proton transformations made possible through the use of a catalyst, in part, to avoid the high energy CO_2 anion radical intermediate.[1] Poor selectivity for the reduction of CO_2 over protons is an inherent challenge associated with such catalytic systems, as the presence of acid is often a requirement for CO_2 reduction.[4-7] Therefore the judicious choice of reaction components and optimization of the catalyst architecture is essential to achieve the desired reactivity and selectivity.

The production of HCOOH from the reduction of CO_2 has applications in many fields, including the textile industry and as a carbon-neutral fuel.[8] CO_2 is abundant, nontoxic, and noncorrosive, properties make it an ideal candidate in industrial applications. Moreover, the high energy density and low flammability of HCOOH under mild conditions are favorable for its safe storage and transport for energy applications.[9-11] It is generally accepted that the metal-catalyzed conversion of CO_2 to HCOOH proceeds *via* CO_2 insertion into a metal-hydride (M–H) bond or hydride transfer from M–H to CO_2, whereas direct CO_2 binding at the active metal center typically results in CO.[12,13] Transition metal complexes of Ru^{II}, $Fe^{II/III}$, Co^{II}, Rh^{III} and Ir^{III} are known to electrocatalytically reduce CO_2 to HCOOH, and in some cases, photochemical activity was achieved in the presence of a sensitizer and a sacrificial donor, however, their selectivity and efficiency vary widely.[14-20] Compared to mononuclear complexes, the presence of a second redox-active metal center in bimetallic complexes is expected to aid multielectron transformations by providing additional low-energy sites available to store redox equivalents.[21-28] Taking advantage of this concept our group has demonstrated that dirhodium complexes are active electrocatalysts for the conversion of CO_2 to HCOOH.[29,30]

Herein, Rh_2(II,II) complexes with varying bridging ligand, L, *cis–H,T*-$[Rh_2(L)_2(phen)_2](BF_4)_2$, where phen = 1,10-phenanthroline and L = trifluoroacetamidate (**1**) or N-tolylacetamidate (**2**), and $[Rh_2(L)_2(phen)_2](BF_4)_2$, where L = N,N'-bis(tolyl)ethanimidamidate (**3**), were prepared and characterized as described in detail in the ESI (Figs. S1 – S12). The structures of **1** – **3** are shown in Fig. 1 and the complexes were explored as electrocatalysts for CO_2 reduction. The cyclic voltammograms (CVs) of **1** – **3** recorded under N_2 in CH_3CN are shown in Fig. 2 and exhibit the first reduction at −0.60 (irr.), −0.80 (ΔEp = 60 mV), and −0.66 (ΔEp = 60 mV) V *vs* Ag/AgCl, respectively. The assignment of this couple as arising from a metal-centered reduction was confirmed through the addition of pyridine, which displaces solvent molecules from the axial site(s) and raises the energy of the $Rh_2(\sigma^*)$ lowest unoccupied molecular orbital (LUMO). Therefore, axial coordination by pyridine is expected to result in a negative shift of the metal-centered reduction events, whereas the position of ligand-based couples should be relatively independent of the identity of the ligand in the axial position(s).[30]

The addition of pyridine to CH_3CN solutions of **1** and **2** revealed a gradual negative shift of the first reduction couple (Fig. S13), consistent with a metal-centered event, Rh_2(II,II/II,I).

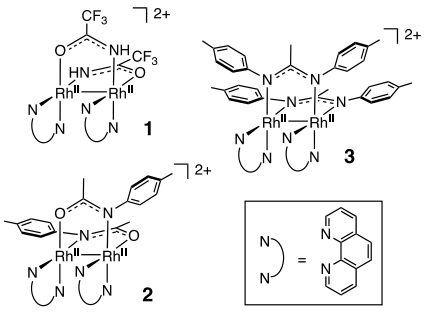

Fig. 1. Schematic representation of the molecular structures of **1** – **3**.

[a] *Department of Chemistry and Biochemistry, The Ohio State University, Columbus, OH 43214, USA.*

Electronic Supplementary Information (ESI) available: [details of any supplementary information available should be included here]. See DOI: 10.1039/x0xx00000x

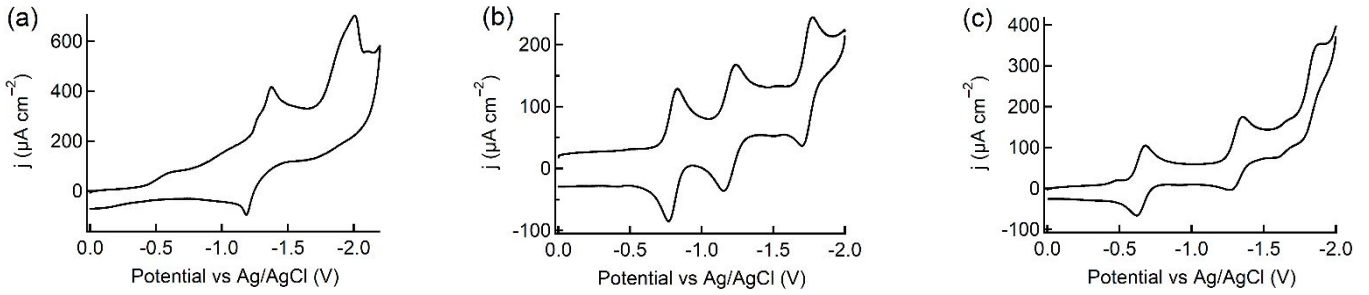

Fig. 2. Cyclic voltammograms of 0.5 mM (a) **1**, (b) **2**, and (c) **3** in CH_3CN (0.1 M $TBAPF_6$) under N_2 (scan rate = 0.1 V/s).

In contrast, the second reduction process in **1** – **3**, observed at −1.28 (quasi-reversible), −1.20 (ΔE_p = 76 mV), and −1.32 V (ΔE_p = 61 mV) *vs* Ag/AgCl, respectively, is independent of the presence of pyridine, such that this couple is assigned as phen$^{0/-}$. The dependence of the phen-centered reduction on the identity of the bridging ligand was previously reported for partial paddlewheel complexes of $DTolF^-$ (p-ditolyl-formamidinate) and mhp^- (anion of 2-methyl-6-hydroxy pyridine), with phen-centered reductions at −1.21 V and −1.05 V *vs* Ag/AgCl respectively.[29,30] A second metal centered Rh_2(II,I/I,I) reduction is observed at −2.00 (irr.), −1.74 (ΔE_p = 70 mV) and −1.83 (ΔE_p = 85 mV) for **1** – **3**, respectively, that is also dependent on the addition of pyridine in **1** and **2**, however, to a lesser extent than the first reduction. The difference in the Rh_2(II,I/I,I) reduction potential between **2** and **3**, 0.11 V, is comparable to that of the Rh_2(II,II/II,I) in these complexes, 0.12 V, consistent with the assignments of these two waves as metal-centered. The three reduction couples measured for **3** are independent of the presence of pyridine, which can be attributed to the greater steric hindrance near the axial sites provided by the presence of two tolyl groups of the bridging ligands, thus preventing axial pyridine coordination.

It is evident from Fig. 2 that the electrochemistry of **1** is sluggish and irreversible, in contrast to the reversible and well-defined couples observed for **2** and **3**. The metal-centered Rh_2(II,II/II,I) reduction places an unpaired electron in the $Rh_2(\sigma^*)$ orbital, resulting in a d^7-d^8 Rh_2(II,I) radical species. In complexes with insufficient steric bulk near the axial positions, the singly occupied $Rh_2(\sigma^*)$ orbitals of two reduced molecules can interact, generating Rh_2–Rh_2 dimers or oligomers. This process can be viewed as a chemical step following the electrochemical step, explaining the irreversible electrochemistry observed with **1**. While similar axial interactions between bimetallic complexes with $(\sigma^*)^2$ and $(\sigma^*)^0$ electron configurations have been previously reported in Rh_2(II,II)/Rh_2(I,I),[31] Pt_2(II,II)/Rh_2(II,II),[32] Ru_2(II,II)/Pt_2(II,II),[33] and Ir_2-Ir_2[34] systems, reports on comparable complexes with half-filled σ* orbitals are rare. One example is the dimerization of bimetallic Pt_2(II,III) d^8–d^7 complexes through their $Pt_2(\sigma^*)^1$ singly-occupied orbitals, resulting in a species with a delocalized unpaired electron known as the "platinum blues".[35,36] In the d^7–d^7 complex $[Rh_2(MeCN)_{10}][BF_4]_4$, similar irreversible reductive electrochemistry was observed,[37] and the reduction product was isolated and characterized as a $[Rh_6(CH_3CN)_{24})]^{9+}$ oligomer featuring two different Rh-Rh distances, 2.9277(8) and 2.8442(8) Å,[38] providing convincing evidence for axial Rh–Rh interactions through the half-filled σ* orbital of each dimer. The presence of bulky tolyl groups near the axial sites in **2** and **3** prevents such interaction, leading to reversible couples (Fig. 2).

Fig. 3 shows the CVs of **1** – **3** recorded in a solution bubbled with N_2 and are compared to those saturated with CO_2 in the absence and presence of H_2O as the proton source to assess the ability of each complex to electrocatalytically reduce CO_2. Complexes **1** – **3** exhibit a significant current enhancement in the presence of CO_2 and 3 M H_2O with an onset at ~–1.4 V *vs* Ag/AgCl in all three complexes (Fig. 3). However, the ~80-fold current enhancement observed for **1** and **2** under CO_2/H_2O is reduced to ~13-fold for **3**.

Since the onset of the catalytic current was observed near −1.4 V *vs* Ag/AgCl, bulk electrolysis for **1** – **3** was conducted at −1.6 V in CH_3CN solutions saturated with CO_2 and 3 M H_2O to characterize the reduction product(s) for each complex and the results are summarized in Table 1. The application of the negative bias to a yellow solution of **1** under CO_2 resulted in a color change to blue with the formation of a blue precipitate within 20 minutes. This precipitation had a negative impact on the rate of charge passed, indicating a decrease in the catalytic process. Similar color change and precipitation were observed in spectroelectrochemical experiments of **1** at –1.0 V *vs* Ag/AgCl under N_2 in the absence of H_2O, which generates the singly-reduced Rh_2 species (Fig. S14). The insoluble species in these experiments is believed to originate from the axial interactions between singly reduced d^7-d^8 Rh_2 units, producing oligomers with poor solubility.[35,36,38,39]

Table 1. Product Distributions and Faradic Efficiencies (%FE) for the Bulk Electrolysis of **1**, **2** and **3** under CO_2 with 3 M H_2O / CH_3CN.[a]

Complex	HCOOH		H_2	
	μmol	%FE	μmol	%FE
1	81(2)	90(3)	1.8(4)	2.0(4)
2	160(6)	93(1)	0.17(6)	0.10(3)
3	16(1)	69(3)	5.2(7)	24(1)

[a][Rh_2] = 0.5 mM; 0.1 M TBAPF6; held at –1.6 V for 1 hour; triplicate runs.

The electrolysis of **2** under CO_2 at −1.6 V *vs* Ag/AgCl, resulted in a color change from yellow to emerald green, without any noticeable formation of insoluble material. Complex **2** exhibits ~2-fold greater CO_2 reduction efficiency as compared to **1**, generating 160 μmol and 81 μmol of HCOOH, respectively (Table 1). The lack of precipitation, along with improved CO_2

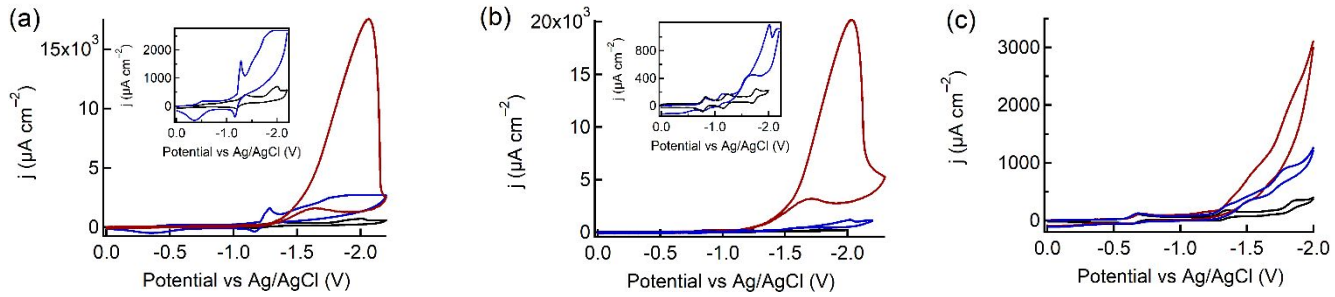

Fig. 3. Cyclic voltammograms of 0.5 mM (a) **1**, (b) **2** and (c) **3** in CH_3CN purged with N_2 (black), CO_2 (blue) and CO_2 in the presence of 3 M H_2O (red) in CH_3CN (scan rate = 0.1 V/s; 0.1 M $TBAPF_6$).

reduction yield is indicative of the inhibition of Rh_2–Rh_2 axial interactions in **2**. However, the electrocatalytic HCOOH formation observed with **1** points to some formation of the active catalytic species along with Rh_2–Rh_2 aggregates.

If indeed the deep blue colored precipitate formed upon reduction of **1** arises from axial interactions between $Rh_2^{II,I}$ units, then one should expect a strong correlation between its formation and the initial concentration of **1**, along with a decrease in HCOOH formation. An opposite trend is expected for **2** and **3**, which do not exhibit axial intermolecular interactions. To test this hypothesis, a series of bulk electrolysis experiments were conducted with varying concentrations of **1**, **2** and **3** in CH_3CN under CO_2 and 3 M H_2O at −1.6 V *vs* Ag/AgCl for 25 min. These experiments revealed an increase in both HCOOH and H_2 formation up to 0.1 mM of **1**, followed by ~30% decrease in product formation with additional increase in complex concentration, consistent with the inhibition of catalysis through Rh_2–Rh_2 aggregation. In contrast, complexes **2** and **3** exhibit a nearly linear increase in HCOOH production with complex concentration up to 1 mM (Fig. S15).

CO_2 reduction assisted by transition metal complexes typically proceeds by CO_2 coordination, which results in the production of CO. The generation of HCOOH generally occurs from a M–H hydride through CO_2 insertion or hydride transfer.[12,13] Vastly different H/D kinetic isotope effect (KIE) values are reported for these mechanisms. Direct CO_2–metal binding results in KIE <2,[40-42] whereas KIE values >2 are expected for reactions that involve M–H bonds.[20,43] CVs were recorded as either H_2O or D_2O was titrated into 0.5 mM solutions of **2** and **3** in CH_3CN under CO_2 (Fig. S16). These experiments reveal KIE values of 5.7 ± 0.1 and 6.1 ± 0.1 for **2** and **3**, respectively. The large KIE values are consistent with hydride transfer from a Rh_2–H hydride intermediate to CO_2 as the rate determining step, as previously reported for Co(II) electrocatalysts.[43]

The application of a −1.6 V *vs* Ag/AgCl bias to a CH_3CN solution of **2** containing 3 M H_2O results in a color change from yellow to emerald green and is accompanied by the appearance of a new absorption feature at ~600 nm both under CO_2 and N_2 (Fig. S17). It should be noted that this peak is not observed when the electrolysis of **2** is conducted at potentials from –1.05 to –1.95 V in the absence of H_2O in CH_3CN, which result in reduction of the complex by one to three electrons (Fig. S17c), or through the formation of the 1e$^-$ or the 2e$^-$ reduced species at −1.05 and −1.45, respectively, in the presence of H_2O in CH_3CN (Figure S17d). These results indicate that the 600 nm spectral feature does not arise from the reduced complex itself and point to the generation of a common species following the 3e$^-$ reduction of **2** in the presence of H_2O that absorbs at ~600 nm under both CO_2 and N_2, likely the Rh_2–H axial hydride. The loss of reversibility and ~0.11 V positive shift of the 2nd reduction event of **2** under CO_2 / 3 M H_2O compared to that under N_2 is indicative of H^+ binding, following the 2e$^-$ reduction of **2** (Fig S18). Therefore, it is expected that protonation of the 2e$^-$ reduced complex, *cis*-$[Rh_2^{II,I}(\mu\text{-L})_2(phen)(phen^-)]^+$, results in the hydride product *cis*-$[H\text{-}Rh_2^{II,III}(\mu\text{-L})_2(phen)(phen^-)]^+$, which can also be written as *cis*- $[H\text{-}Rh_2^{II,II}(\mu\text{-L})_2(phen)(phen)]^+$ if one considers an electron transfer from reduced phen ligand to the dirhodium core upon hydride formation. It is proposed that this species must undergo another one-electron reduction to generate the active intermediate *cis*-$[H\text{-}Rh_2^{II,I}(\mu\text{-L})_2(phen)_2]^0$. The slow chemical reaction between *cis*-$[H\text{-}Rh_2^{II,I}(\mu\text{-L})_2(phen)_2]^0$ and CO_2 suggested by the observed KIE values, allows the accumulation of the Rh_2(II,I)–H hydride species in solution, with an absorption at ~600 nm.

Similar electrolysis experiments were conducted with **3** in CH_3CN under CO_2 and N_2 at −1.6 V, which resulted in the growth of absorption features at ~445 and ~540 nm, both in the presence and absence of 3 M H_2O (Fig. S19). Unlike the formation of the hydride following the reduction of **2**, the spectral features observed for **3** likely arise from the three-electron reduced complex. The absence of spectral features associated with a Rh_2-H hydride species in the case of **3** points to a slow reaction between reduced Rh_2 and H^+. The possibility that the Rh_2–H reacts rapidly with CO_2 or protons precluding its accumulation can be ruled out by the low electrocatalytic yields of HCOOH and H_2 obtained with **3**.

In conclusion, the combined results suggest that, at −1.6 V, **2** is reduced by three electrons and it is protonated in the presence of H_2O to form the axial $Rh_2^{II,I}$–H hydride that was detected as a persistent intermediate with an absorption at ~600 nm, which transfers a hydride to CO_2 and releases HCOOH upon protonation (Fig. 4).[43,44] As depicted in Fig. 4, **1** is inactivated by oligomer formation upon reduction. Complex **3** exhibits the least reactivity and selectivity for CO_2 reduction. Complexes **2** and **3** possess one and two tolyl groups that block each axial site, respectively. Therefore, the lower reactivity of **3** can be attributed to the increased steric hindrance closer the catalytically active axial sites.

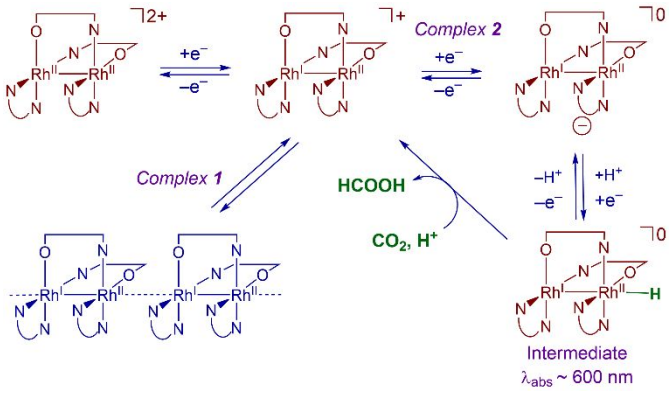

Fig. 4. Proposed electrocatalytic cycle for CO_2 to HCOOH conversion with **1** and **2**.

The authors thank the support from the Department of Energy, Office of Science, Office of Basic Energy Sciences (DESC0020243), and The Ohio State University for partial support of this work.

Conflicts of Interest

There are no conflicts to declare.

Notes and references

1. C. Costentin, M. Robert and J.-M. Savéant, *Chem. Soc. Rev.*, 2013, **42**, 2423-2436.
2. C. D. Windle and R. N. Perutz, *Coord. Chem. Rev.*, 2012, **256**, 2562-2570.
3. J. L. Inglis, B. J. MacLean, M. T. Pryce and J. G. Vos, *Coord. Chem. Rev.*, 2012, **256**, 2571-2600.
4. S. Gonell, M. D. Massey, I. P. Moseley, C. K. Schauer, J. T. Muckerman and A. J. M. Miller, *J. Am. Chem. Soc.*, 2019, **141**, 6658-6671.
5. A. J. Morris, G. J. Meyer and E. Fujita, *Acc. Chem. Res.*, 2009, **42**, 1983-1994.
6. J. Bonin, A. Maurin and M. Robert, *Coord. Chem. Rev.*, 2017, **334**, 184-198.
7. R. Hegner, L. F. M. Rosa and F. Harnisch, *Appl. Catal., B*, 2018, **238**, 546-556.
8. S. Moret, P. J. Dyson and G. Laurenczy, *Nat. Commun.*, 2014, **5**, 4017.
9. J. Eppinger and K.-W. Huang, *ACS Energy Lett.*, 2017, **2**, 188-195.
10. A. Taheri and L. A. Berben, *Chem. Commun.*, 2016, **52**, 1768-1777.
11. K. M. Waldie, F. M. Brunner and C. P. Kubiak, *ACS Sustainable Chem. Eng.*, 2018, **6**, 6841-6848.
12. C. W. Machan, M. D. Sampson and C. P. Kubiak, *J. Am. Chem. Soc.*, 2015, **137**, 8564-8571.
13. N. Elgrishi, M. B. Chambers, X. Wang and M. Fontecave, *Chem. Soc. Rev.*, 2017, **46**, 761-796.
14. C. M. Bolinger, B. P. Sullivan, D. Conrad, J. A. Gilbert, N. Story and T. J. Meyer, *J. Chem. Soc., Chem. Commun.*, 1985, 796-797.
15. C. Caix, S. Chardon-Noblat and A. Deronzier, *J. Electroanal. Chem.*, 1997, **434**, 163-170.
16. Y. Kuramochi, J. Itabashi, K. Fukaya, A. Enomoto, M. Yoshida and H. Ishida, *Chem. Sci.*, 2015, **6**, 3063-3074.
17. P. Kang, C. Cheng, Z. Chen, C. K. Schauer, T. J. Meyer and M. Brookhart, *J. Am. Chem. Soc.*, 2012, **134**, 5500-5503.
18. S.-N. Pun, W.-H. Chung, K.-M. Lam, P. Guo, P.-H. Chan, K.-Y. Wong, C.-M. Che, T.-Y. Chen and S.-M. Peng, *J. Chem. Soc., Dalton Trans.*, 2002, 575-583.
19. L. Chen, Z. Guo, X.-G. Wei, C. Gallenkamp, J. Bonin, E. Anxolabéhère-Mallart, K.-C. Lau, T.-C. Lau and M. Robert, *J. Am. Chem. Soc.*, 2015, **137**, 10918-10921.
20. S. Roy, B. Sharma, J. Pécaut, P. Simon, M. Fontecave, P. D. Tran, E. Derat and V. Artero, *J. Am. Chem. Soc.*, 2017, **139**, 3685-3696.
21. T. S. Teets, T. R. Cook, B. D. McCarthy and D. G. Nocera, *J. Am. Chem. Soc.*, 2011, **133**, 8114-8117.
22. T. S. Teets, T. R. Cook, B. D. McCarthy and D. G. Nocera, *Inorg. Chem.*, 2011, **50**, 5223-5233.
23. H. Zhang, G. P. Hatzis, C. E. Moore, D. A. Dickie, M. W. Bezpalko, B. M. Foxman and C. M. Thomas, *J. Am. Chem. Soc.*, 2019, **141**, 9516-9520.
24. A. M. Poitras, M. W. Bezpalko, C. E. Moore, D. A. Dickie, B. M. Foxman and C. M. Thomas, *Inorg.Chem.*, 2020, **59**, 4729-4740.
25. R. B. Siedschlag, V. Bernales, K. D. Vogiatzis, N. Planas, L. J. Clouston, E. Bill, L. Gagliardi and C. C. Lu, *J. Am. Chem. Soc.*, 2015, **137**, 4638-4641.
26. J. T. Moore, S. Chatterjee, M. Tarrago, L. J. Clouston, S. Sproules, E. Bill, V. Bernales, L. Gagliardi, S. Ye, K. M. Lancaster and C. C. Lu, *Inorg.Chem.*, 2019, **58**, 6199-6214.
27. J. T. Moore and C. C. Lu, *J. Am. Chem. Soc.*, 2020, **142**, 11641-11646.
28. Y. Kataoka, N. Yano, M. Handa and T. Kawamoto, *Dalton Trans.*, 2019, **48**, 7302-7312.
29. S. E. Witt, T. A. White, Z. Li, K. R. Dunbar and C. Turro, *Chem. Commun.*, 2016, **52**, 12175-12178.
30. H. D. Manamperi, S. E. Witt and C. Turro, *ACS Appl. Energy Mater.*, 2019, **2**, 7306-7314.
31. F. A. Cotton, E. V. Dikarev and M. A. Petrukhina, *J. Organomet. Chem.*, 2000, **596**, 130-135.
32. K. Uemura and M. Ebihara, *Inorg. Chem.*, 2011, **50**, 7919-7921.
33. K. Uemura, N. Uesugi, A. Matsuyama, M. Ebihara, H. Yoshikawa and K. Awaga, *Inorg. Chem.*, 2016, **55**, 7003-7011.
34. C. Tejel, M. A. Ciriano, B. E. Villarroya, J. A. López, F. J. Lahoz and L. A. Oro, *Angew. Chem. Int. Ed.*, 2003, **42**, 529-532.
35. J. K. Barton, H. N. Rabinowitz, D. J. Szalda and S. J. Lippard, *J. Am. Chem. Soc.*, 1977, **99**, 2827-2829.
36. J. K. Barton, D. J. Szalda, H. N. Rabinowitz, J. V. Waszczak and S. J. Lippard, *J. Am. Chem. Soc.*, 1979, **101**, 1434-1441.
37. K. R. Dunbar, L. E. Pence, J. Czuchajowska, F. A. Cotton, *Inorg. Synth.*, 1992, **29**, 182-185.
38. G. M. Finniss, E. Canadell, C. Campana and K. R. Dunbar, *Angew. Chem. Int. Ed.*, 1996, **35**, 2772-2774.
39. J. Xie, C. Li, Q. Zhou, W. Wang, Y. Hou, B. Zhang and X. Wang, *Inorg. Chem.*, 2012, **51**, 6376-6384.
40. S. E. Tignor, T. W. Shaw and A. B. Bocarsly, *Dalton Trans.*, 2019, **48**, 12730-12737.
41. A. Chapovetsky, M. Welborn, J. M. Luna, R. Haiges, T. F. Miller and S. C. Marinescu, *ACS Central Science*, 2018, **4**, 397-404.
42. J. M. Smieja, E. E. Benson, B. Kumar, K. A. Grice, C. S. Seu, A. J. M. Miller, J. M. Mayer and C. P. Kubiak, *Proc. Natl. Acad. Sci. U.S.A.*, 2012, **109**, 15646.
43. S. Roy, B. Sharma, J. Pecaut, P. Simon, M. Fontecave, P. D. Tran, E. Derat and V. Artero *J. Am. Chem. Soc.*, 2017, **139,** 3685-3696.
44. D. W. Cunningham and J. Y. Yang *Chem. Commun.* 2020, **56**, 12965-12968.